Postnatal Elongation of Eye Size in DBA/2J Mice Compared with C57BL/6J Mice: In Vivo Analysis with Whole-Eye OCT

Tsung-Han Chou,[1,2] *Omer P. Kocaoglu,*[1,2] *David Borja,*[1,2] *Marco Ruggeri,*[1,2] *Stephen R. Uhlhorn,*[1,2] *Fabrice Manns,*[1,2] *and Vittorio Porciatti*[1]

Purpose. To characterize postnatal changes in eye size in glaucomatous DBA/2J (D2) mice and in nonglaucomatous C57BL/6J mice (B6) in vivo by means of whole-eye optical coherence tomography (OCT).

Methods. D2 (n = 32) and B6 (n = 36) mice were tested between 2 and 20 months of age in eight age bins. A custom time-domain OCT system with a center wavelength of 825 nm and an axial scan length of 7.1 mm produced axial A-scan interferograms at a rate of 20 A-lines/s with a resolution of 8 μm. Axial length (AL), corneal thickness (CT), anterior chamber depth (ACD), lens thickness (LT), vitreous chamber depth (VCD), and retinal thickness (RT) were measured in the optical axis and adjusted with corresponding refractive indices. Corneal curvature (CC) and IOP were also measured.

Results. AL increased ($P < 0.001$) more in the D2 (21%) than in the B6 (9%) mice. There was an interaction effect (two-way ANOVA, $P < 0.001$) between age and strain for AL, CT, ACD, and VCD. In the D2 mice, the lens became dislocated posteriorly. Multiple regression analysis in the D2 mice revealed an independent effect of age and IOP ($P \leq 0.01$) on axial length. CC steepened in the older D2 mice, whereas it flattened in the B6 mice.

Conclusions. In D2 mice, postnatal elongation of AL is larger than that in B6 mice and is associated with a greater increase in ACD and IOP, which seems to be a causal factor. The ease of use, short acquisition time, and noninvasiveness of whole-eye OCT make it suitable for routine use in longitudinal studies of mouse models. (*Invest Ophthalmol Vis Sci.* 2011;52:3604–3612) DOI:10.1167/iovs.10-6340

The mouse is the most widely used animal model of human diseases, including inherited vision disorders.[1–6] The eye is known to undergo substantial postnatal elongation that continues beyond the period of sexual maturity.[7,8] Normal postnatal eye elongation may be substantially altered by manipulating the environmental conditions—for example, manipulating refraction to induce myopia[9] or intraocular pressure (IOP) to induce glaucoma.[4,10] It is therefore important to monitor postnatal changes in eye size, including relative changes of individual components, to retrieve relevant information to determine the refractive properties of the eye for vision testing and for a better understanding of the disease process.

Ultrasound,[11–13] magnetic resonance imaging,[14–19] and optical low-coherence biometry[13,20,21] have been used to measure intraocular distance or dimensions of rat and mouse eyes in vivo. These techniques may not be optimal for routine assessment of mouse models in large-scale longitudinal studies. Repeatable measurements are relatively difficult to acquire with ultrasound because of the small size of the mouse eye and resolution limits. Magnetic resonance imaging (MRI) is expensive and requires a long imaging time. Optical low-coherence biometry provides distances along a single direction but cannot measure parameters such as radius of curvature. Zhou et al.[22] used optical coherence tomography (OCT) with a focal-plane–advancement technique to acquire images of the whole mouse eye. Whole-eye images were reconstructed by stitching together sequential images acquired at different depths. The approach is relatively slow (1.5 minutes per image) and requires substantial postprocessing.

To noninvasively monitor postnatal changes of the mouse eye size over time, we have developed a time-domain OCT system capable of whole-eye imaging.[23] The instrument has a beam-delivery system with sufficient depth of focus and resolution to provide reliable measurements of individual eye components along the entire eye axis.

We used this whole-eye OCT system to quantify postnatal changes in axial eye components and in corneal curvature (CC), in the well-established DBA/2J (D2) mouse model of spontaneous IOP elevation and glaucoma.[11,24,25] In the model, the eye perimeter has been determined by manganese-enhanced MRI to be abnormally enlarged in older mice.[17] We compared postnatal changes in eye components in D2 mice with corresponding changes occurring in C57BL/6J (B6) mice, a common control mouse that does not develop IOP elevation or any other abnormal eye condition. Preliminary results of this study have been reported in abstract form (Chou T-H, et al. *IOVS* 2009;50:ARVO E-Abstract 2776; Manns F, et al. *IOVS* 2009;50:ARVO E-Abstract 5670; Ruggeri M, et al. *IOVS* 2002; 43:ARVO E-Abstract 6363).

Methods

Animals and Husbandry

This study was approved by the Animal Care and Use Committee at University of Miami. All experiments were conducted according to the ARVO Statement for the Use of Animals in Ophthalmic and Vision

From the [1]Bascom Palmer Eye Institute, University of Miami, Miller School of Medicine, Miami, Florida; and the [2]Department of Biomedical Engineering, University of Miami, Coral Gables, Florida.

Supported by National Institutes of Health (NIH) Grants R01-EY019077 (VP), P30-EY14801 (VP), and F32-EY15636 (SRU); and an unrestricted grant to Bascom Palmer Eye Institute from Research to Prevent Blindness.

Submitted for publication August 4, 2010; revised November 16 and December 23, 2010; accepted January 5, 2011.

Disclosure: **T.-H. Chou**, None; **O.P. Kocaoglu**, None; **D. Borja**, None; **M. Ruggeri**, None; **S.R. Uhlhorn**, None; **F. Manns**, None; **V. Porciatti**, None

Corresponding author: Vittorio Porciatti, Bascom Palmer Eye Institute, University of Miami, Miller School of Medicine, 900 NW 17th Street, Miami, FL 33136; vporciatti@med.miami.edu.

Research. C57BL/6J mice (B6) and DBA/2J mice (D2), either 2 or 8 months old, were purchased (Jackson Laboratory, Bar Harbor, ME). They were aged in our AAALAC-certified vivarium in a standard 12:12-hour light–dark cycle and fed a grain-based diet (Rodent Opti-diet 500; LabDiet, St. Louis, MO). The mice were tested in eight age bins in the age range 2 to 20 months. The age bins were in intervals of 2 months below 1 year of age and 3 months after 1 year of age: 2 to 3; 4 to 5; 6 to 7; 8 to 9; 10 to 11; 12 to 14; 15 to 17; and 18 to 20. Altogether, we were able to obtain outcome measurements in 32 D2 mice and 36 B6 mice in the age range 2 to 20 months.

The mice were weighed and anesthetized with IP injections (0.5–0.7 mL/kg) of a mixture of ketamine 42.8 mg/mL and xylazine 8.6 mg/mL. Under these conditions, the eyes of mice are naturally wide open and in a stable position, with pupils pointing laterally and upward. As pupils in older D2 mice cannot be dilated pharmacologically—possibly due to both stromal atrophy and the presence of synechiae[11]—to normalize our approach, we decided not to dilate the pupil in any mouse. After IOP and OCT testing, the mice were allowed to recover from anesthesia and put back in their cages.

Time-Domain OCT System

A time-domain OCT system with an axial scanning range of 10 mm in air (~7 mm in tissue) was used (Fig. 1). The time domain OCT system is described in detail elsewhere.[26] It incorporates a superluminescent diode with a center wavelength of 825 nm, a bandwidth of 25 nm, and a maximum output power of 6 mW (SLD-38-HP; Superlum, Cork, Ireland). The reference arm of the OCT interferometer is a linear delay line with a corner cube retroreflector. The axial resolution in tissue is 8 μm and the system sensitivity is 85 dB. The beam-delivery system has an *X–Y* galvanometer scanning system followed by an achromatic lens with a focal length of 100 mm, to provide a telecentric scan with a flat field and large depth of focus. The focal length was calculated so that the depth of focus nearly matched the axial scan length of the OCT system (10 mm in air). The OCT beam spot diameter at the focus was 60 μm. Images were recorded with 5000 points per A-line and 500 A-lines per frame at a rate of 20 A-lines/s. Image acquisition speed was limited by the scanning speed of the linear delay line and its long scanning distance. The total image acquisition time was on the order of 25 seconds per B-scan image.

Imaging Technique

The anesthetized animal was placed in a custom-made cylindrical holder and mounted on a custom-made mouse-positioning stage developed in our laboratory (Fig. 1).[27] A single operator adjusted the position of the animal. An infrared sensor card was first used to visualize the OCT beam and position the animal so that the beam was roughly incident on the center of the cornea. The mouse position was then adjusted, with a real-time display of the central A-line used for guidance, until the intensity peaks corresponding to the cornea, lens, and retina were detected and maximized. Final alignment was then performed by using a near–real-time, low-density B-scan image for guidance. The eye was considered to be aligned when the intensity of the anterior cornea, posterior lens, and anterior retinal surfaces in the low-density B-scan were maximized. Multiple cross-sectional OCT images were then acquired along parallel planes situated at different positions around the pupil center. In all experiments, the cornea was irrigated at regular intervals through a cannula filled with balanced salt solution (BSS; Alcon, Fort Worth, TX), to avoid dehydration and loss of transparency. Any fluid accumulated on the ocular surface was gently removed with a microsponge before each image acquisition. The absence of the fluid layer was confirmed on the OCT images. At the end of the imaging session, the animal was returned to its cage. From the time the animal was placed on the positioning stage, each imaging session took approximately 10 to 15 minutes, including the positioning time and multiple image acquisition at different positions.

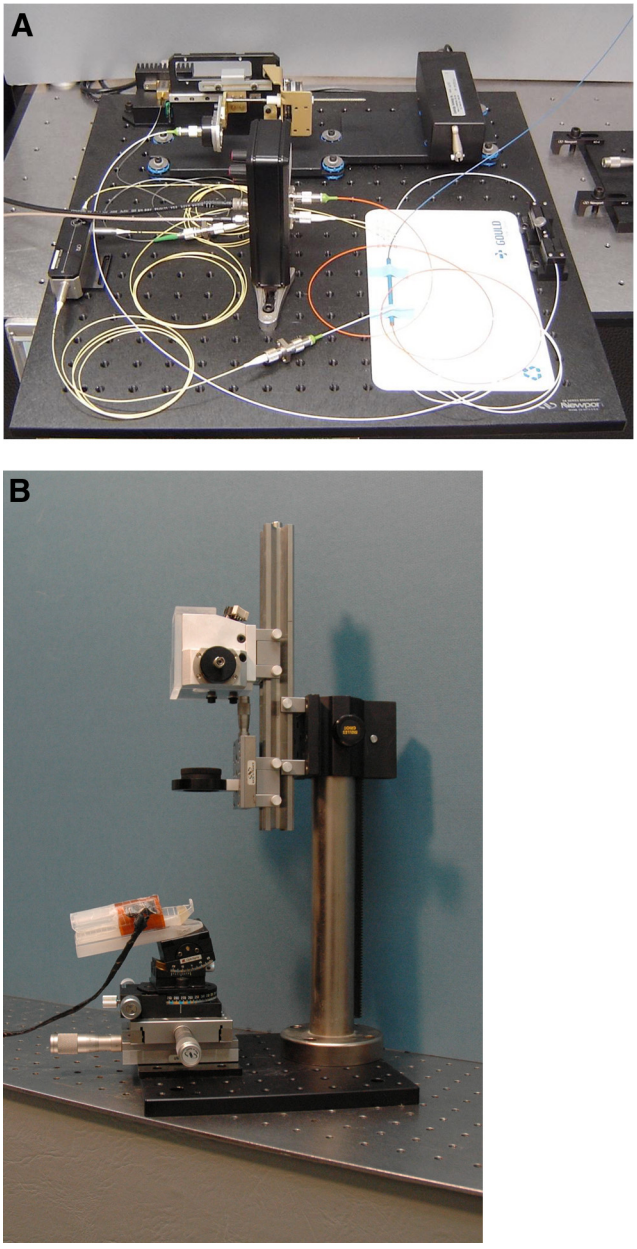

FIGURE 1. (**A**) Time-domain OCT interferometer and (**B**) table-top delivery system with mouse-positioning stage.

Biometry

All distances and shapes were measured on the B-scan image passing through the center of the pupil. This image was identified as the image where the pupil diameter was the largest. Some of the older D2 mice had eccentric pupils. However, scattered loss of iris pigment allowed sufficient light transmission through the iris to generate detectable signals from the lens and retinal boundaries posterior to the iris along or close to the eye axis, which we used for axial length measurements.

A semiautomated, customized edge-detection algorithm was developed to segment the images and measure anterior corneal shape, posterior corneal shape, corneal thickness (CT), anterior chamber depth (ACD), lens thickness (LT), vitreous chamber depth (VCD), retinal thickness (RT), and axial length (AL) (Fig. 2). The corneal surfaces were fitted with conic sections to calculate the radius of curvature and asphericity (Fig. 2). Ocular distances were measured along the A-line passing through the center of the pupil. Optical distances were converted to geometric distances using published val-

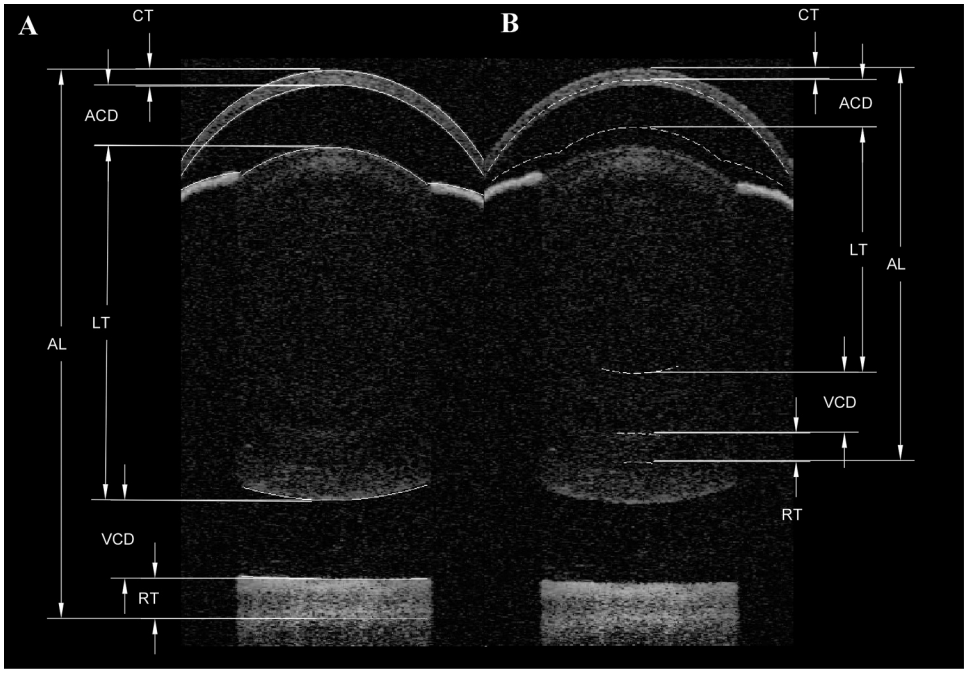

FIGURE 2. Representative in vivo OCT image of the whole eye of a C57BL/6J mouse. The cornea, anterior chamber, and iris and portions of the lens, vitreous, and retina that are not blocked by the iris can be clearly visualized. The images show the distance measurements after segmentation with automated edge detection before (**A**) and after (**B**) correction for image refractive distortion.

ues of the refractive indices at 655 nm of the mouse cornea (1.4015), aqueous (1.3336), and vitreous (1.3329).[28] These values were not adjusted for dispersion or converted from phase to group index, because there are no published data on the dispersion of the mouse ocular media in near-infrared. From an analysis of the dispersion of human ocular media, we estimate that the relative error in the distances introduced by this approximation is less than 1%. An average refractive index of 1.45 was used for the lens. The value was estimated by assuming that the mouse lens is spherical with a parabolic index with core (1.50) and surface values (1.39) equal to those of the rat lens.[29] A refractive index 1.38 was assumed for the retina. AL was measured from the corneal surface to the pigment epithelium and corresponded to the summed thicknesses of all eye components: CT, ACD, LT, VCD, and RT (details in Fig. 2). The variability of measurements between two imaging sessions, quantified in one 8-month-old B6 mouse, was less than 5% for all distances. Potential measurement errors due to alignment were estimated on another 8-month-old B6 mouse by taking four additional images with the animal positioned at 0.1 and 0.2 mm from the initial aligned position. For each intraocular distance, the measurement error was estimated by calculating the difference between the minimum and maximum values of the five measurements and dividing the result by the mean of the five measurements. The relative error was less than 10% for all distances except for the RT, with an error of 16% (32 μm).

To quantify anterior and posterior CC, we used a semiautomated edge-detection program developed for mouse ocular biometry.[23] The program detects the ocular surface boundaries and performs a conic section fit to calculate the radius of curvature and asphericity of each surface. The program also uses a ray-tracing algorithm to correct image distortions due to refraction. Typical examples showing the uncorrected and corrected conic section fits of ocular boundaries are shown in Figure 2.

IOP Measurement

IOP readings were obtained with rebound tonometer (TonoLab; Icare, Helsinki, Finland), [30] which has been shown to be accurate and reproducible in different mouse strains including DBA/2J[31–35] The tonometer was fixed in a vertical position to a support stand by means of clamps. Anesthetized mice were placed on an adjustable stand. The probe tip was aligned with the optical axis of the eye at 1 to 2 mm distance with a magnifier lamp. The instrument takes six individual measurements to display one IOP reading. Five consecutive IOP readings were obtained and averaged in each eye.

Analysis

OCT and IOP measurements were performed in both eyes, and average values were used as a single entry for statistical calculations. Two-way ANOVA was performed to test the hypothesis that the size of eye components changes with age and also to determine whether age-related changes are different in the two strains. Multiple correlations (Pearson's) were performed to evaluate the strength of the associations between eye components and IOP. Multiple linear regression analysis was performed to evaluate whether age and IOP have independent effects on AL.

RESULTS

Figure 3 shows representative examples of whole-eye OCT recorded in the D2 and B6 mice at different ages. The imaging system successfully acquired whole-eye images in all animals that clearly show the boundaries that are not obscured by the iris, including the cornea, anterior chamber, lens, anterior iris, vitreous, and retina. Figure 4 provides summary plots of changes in the mean size of all ocular components as a function of increasing age. Actual sizes at specific ages for each eye component are reported in Tables 1 and 2, together with the significance of age-related changes (one-way ANOVA). Overall comparisons between the D2 and B6 mice were tested with two-way ANOVA. The main effects tested were, strain (size differs between the D2 and B6 mice), age (size changes with age), and interaction between strain and age (age-related changes are different between the D2 and B6 mice.

It is readily apparent in Figures 3 and 4 that in young mice (2–5 months) the AL was similar in the D2 and B6 mice and tended to grow in parallel with increasing age. At older ages, however, the AL increased relatively more in the D2 than in the B6 mice, until it leveled off between 10 and 20 months of age. The plateau AL in the D2 mice was approximately 23% larger than that at 2 to 3 months in the D2 mice (as opposed to ~9% in the B6 mice). This differences were significant (two-way

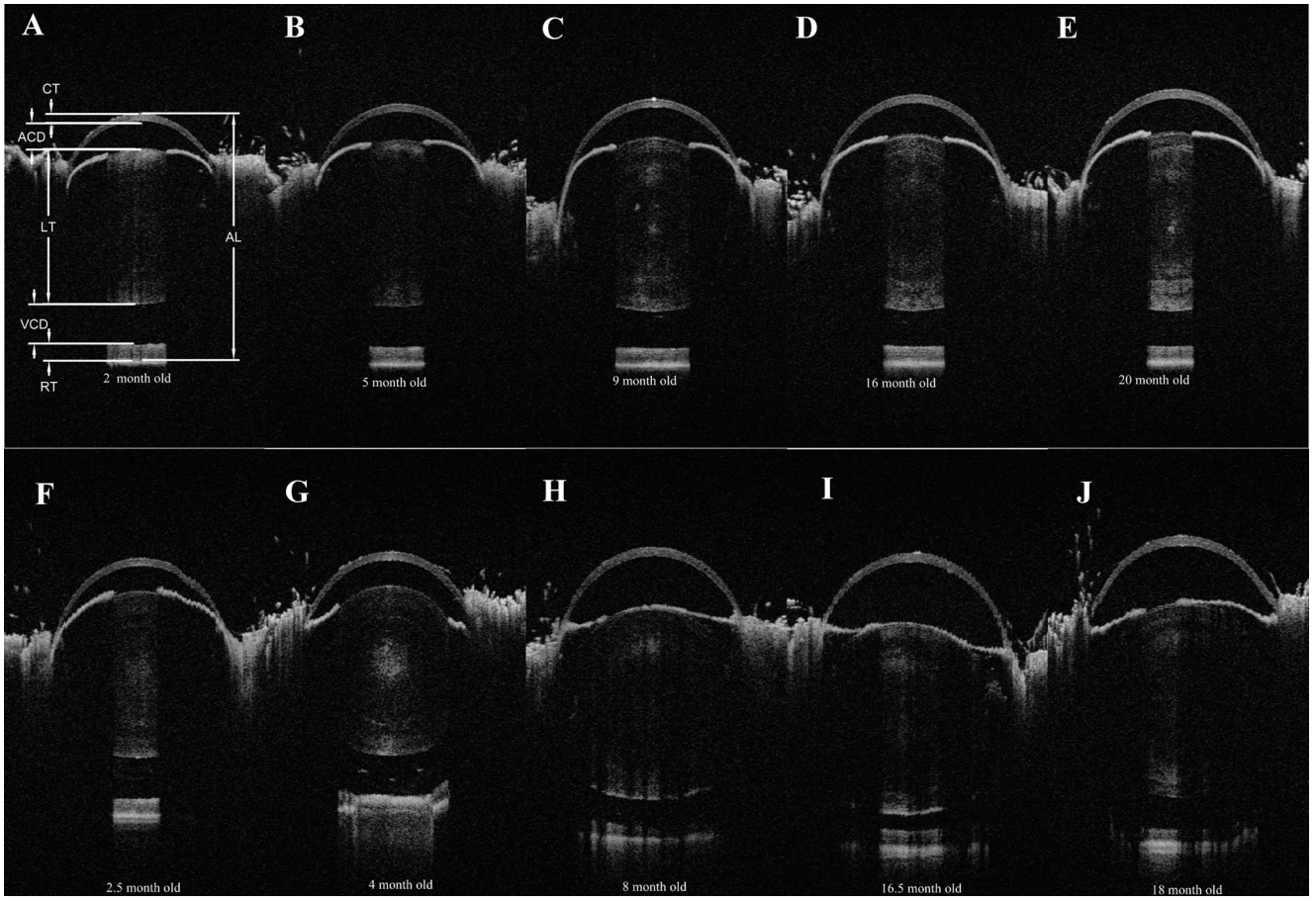

FIGURE 3. Shown are representative examples of whole-eye OCT images recorded in C57BL/6J mice aged 2 (**A**), 5 (**B**), 9 (**C**), 16 (**D**), and 20 (**E**) months and corresponding representative examples for DBA/2J mice aged 2.5 (**F**), 4 (**G**), 8 (**H**), 16.5 (**I**), and 18 (**J**) months. Note irregularities of the iris signal due to depigmentation in older mice (**H–J**) that cause image discontinuity in the lens and retina.

ANOVA: strain, $F_{(1,65)} = 142.9$, $P < 0.001$; age, $F_{(7,65)} = 40.1$, $P < 0.001$; and age × strain, $F_{(7,65)} = 11.3$, $P < 0.001$).

The effects described for AL were reflected to some extent in all eye components, albeit with some notable differences. The CT tended to increase with age in both strains (ANOVA, $P < 0.001$). In the B6 mice the increase was progressive (~16% between 18–20-month-old and 2–3 month old mice), whereas in the D2, mice it was more irregular, with a sharp peak/trough at 8 to 10 months, eventually reaching a value approximately 60% larger than the 2- to 3-month baseline. This change in CT was significant (two-way ANOVA: strain, $F_{(1,65)} = 16.4$, $P < 0.001$; age $F_{(7,65)} = 11.57$, $P < 0.001$; and age × strain, $F_{(7,65)} = 5.85$, $P < 0.001$).

The ACD tended to increase with age in both strains, but in the D2 mice the postnatal elongation of the anterior chamber was much larger, up to ~128% larger than the 2- to 3-month-old baseline (as opposed to ~18% in the B6 mice). This effect was significant (two-way ANOVA: strain, $F_{(1,65)} = 211.8$, $P < 0.001$; age, $F_{(7,65)} = 38.7$, $P < 0.001$; and age × strain, $F_{(7,65)} = 24.49$, $P < 0.001$).

LT increased with age in both the D2 and B6 mice with a very similar time course. However, at all ages, the lens was thicker in the D2 than in the B6 mice by approximately 5%. Two-way ANOVA was significant for strain, $F_{(1,65)} = 47.9$, $P < 0.001$; age $F_{(7,65)} = 27.13$, $P < 0.001$; but not for age × strain, $F_{(7,65)} = 0.67$, $P = 0.7$.

The VCD tended to decrease progressively with age in both strains (ANOVA, $P < 0.001$), eventually reaching a shorter depth by approximately 16% in the B6 mice and by approximately 36% in the D2 mice compared with the 2- to 3-month baseline. Although in the B6 mice the age-related decrease in VCD was fairly progressive, in the D2 mice VCD data measurements showed a more complex course. In particular, at ~8 months of age there was an abrupt decrease in VCD. This finding is unlikely to be artifactual, as this decrease in VCD was consistent and always associated with a corresponding increase in the ACD, of the same but opposite amount. Two-way ANOVA revealed significant changes in VCD with increasing age $F_{(7,65)} = 7.06$, $P < 0.001$; and age × strain, $F_{(7,65)} = 4.7$, $P < 0.001$; but not with strain, $F_{(1,65)} = 0.87$, $P = 0.35$.

The RT did not change significantly with increasing age in both strains, although there was a trend toward decreased thickness. At all ages, the RT was on average thinner in the D2 mice than in the B6 mice by approximately 8%. Two-way ANOVA revealed significant differences in RT with increased strain, $F_{(1,65)} = 7.3$, $P = 0.014$; but not with age $F_{(7,65)} = 0.55$, $P = 0.62$; or age × strain, $F_{(7,65)} = 1.05$, $P = 0.75$.

Figure 4 also includes two relevant variables associated with eye elongation: body weight and IOP. In both the B6 and D2 mice, body weight increased rapidly between 2 and 6 months and then plateaued at a level approximately 12% higher in the D2 mice than in the B6 mice. Two-way ANOVA revealed significant changes in IOP with increasing age, $F_{(7,65)} = 34.08$, $P < 0.001$; strain, $F_{(1,65)} = 28.04$, $P < 0.001$; and age × strain, $F_{(7,65)} = 8.0$, $P < 0.001$.

In both the B6 and the D2 mice, IOP tended to increase between 2 and 6 months. In the B6 mice, IOP plateaued at ~20

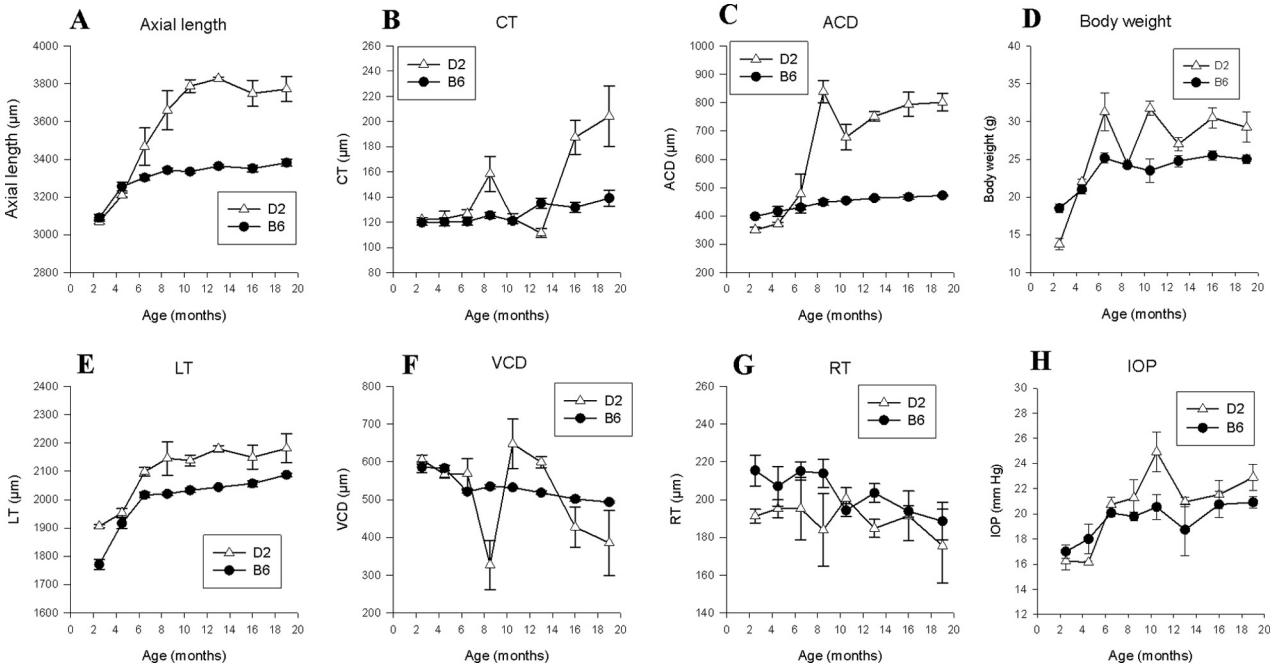

FIGURE 4. Changes of axial ocular components with age in DBA/2J and C57BL/6J mice. (**A**) AL, (**B**) CT, (**C**) ACD, (**E**) LT, (**F**) VCD, and (**G**) RT, measured by time-domain, whole-eye OCT. Changes in body weight (**D**) and IOP (**H**) are also displayed. In each panel, the data points represent the mean ± SEM.

mm Hg, whereas in the D2 mice, it continued to increase with age, reaching a peak at ~10 months of age and plateauing at a level higher than in the B6 mice. Two-way ANOVA revealed significant changes in IOP with increasing age, $F_{(7,65)} = 8.92$, $P < 0.001$; and strain, $F_{(1,65)} = 4.83$, $P = 0.032$; but not with age × strain, $F_{(7,65)} = 1.62$, $P = 0.15$.

Figure 5 displays scattergrams relating individual IOP data with corresponding dimensions of relevant eye components that are expected to be altered by IOP elevation. Body weight is also shown, as it is associated with age-dependent IOP changes. The major feature of Figure 5 is that for all variables, the regression slopes appeared relatively steeper in the D2 mice than in the B6 mice. For both the D2 and B6 mice, all regressions were significant at $P < 0.05$ or higher, albeit relatively stronger for the D2 mice. No obvious associations between highest IOPs and dimensions of eye components were observable.

To test the hypothesis that IOP plays a role in AL elongation, we included covariate anatomic variables in a multiple-regression model. The model tested the prediction that AL depends on a linear combination of the independent variables strain, age, body weight, IOP, CT, ACD, LT, VCD, and RT. For the categorical strain variable, a nominal value of 1 for the D2 mice and 2 for the B6 mice was arbitrarily chosen. Among the several independent variables, AL was best predicted by the independent variables strain ($P < 0.001$), age ($P < 0.001$), and IOP ($P = 0.001$), according to the equation: AL (in micrometers) = 3041.777 (229.76 × strain) + (26.23 × age [months] +

TABLE 1. Dimensions of Eye Components in D2 and B6 Mice Aged 2.5 to 19 Months

	n	CT	ACD	LT	VCD	RT	AL
D2 Age Groups							
2–3	4	122 ± 9	351 ± 27	1906 ± 29	606 ± 37	191 ± 13	3069 ± 43
4–5	4	123 ± 9	372 ± 27	1953 ± 29	567 ± 37	195 ± 11	3209 ± 43
6–7	4	127 ± 9	478 ± 27	2098 ± 29	569 ± 37	195 ± 11	3467 ± 43
8–9	4	158 ± 7	837 ± 27	2146 ± 23	327 ± 31	184 ± 9	3660 ± 43
10–11	4	123 ± 9	678 ± 27	2138 ± 29	648 ± 37	201 ± 11	3787 ± 43
12–14	4	111 ± 9	752 ± 27	2180 ± 29	600 ± 37	185 ± 11	3827 ± 43
15–17	4	188 ± 9	794 ± 27	2150 ± 29	427 ± 37	191 ± 11	3749 ± 43
18–20	4	204 ± 9	801 ± 27	2181 ± 33	385 ± 43	175 ± 13	3771 ± 50
B6 Age Groups							
2–3	6	120 ± 7	398 ± 22	1771 ± 23	586 ± 31	215 ± 9	3089 ± 45
4–5	3	120 ± 10	416 ± 27	1917 ± 33	583 ± 43	207 ± 13	3256 ± 37
6–7	6	121 ± 7	430 ± 22	2016 ± 23	521 ± 31	215 ± 9	3303 ± 36
8–9	5	126 ± 8	448 ± 24	2020 ± 26	534 ± 33	214 ± 10	3342 ± 23
10–11	4	121 ± 9	454 ± 27	2033 ± 29	532 ± 37	194 ± 11	3335 ± 24
12–14	4	135 ± 9	463 ± 27	2044 ± 29	518 ± 37	203 ± 11	3363 ± 19
15–17	4	132 ± 9	467 ± 27	2057 ± 29	502 ± 37	194 ± 11	3353 ± 30
18–20	3	139 ± 10	472 ± 31	2087 ± 33	494 ± 43	189 ± 13	3388 ± 31

Data are expressed in micrometers (mean ± SD).

TABLE 2. Comparison of Ocular Dimensions in B6 and D2 Mice of Different Ages between Different Laboratories and Instruments

Study (Mouse Age)	Method	CT	ACD	LT	VCD	RT	AL
B6, 2–3 Months							
Present results	OCT	120 ± 7	398 ± 22	1771 ± 23	586 ± 31	215 ± 9	3089 ± 45
Schmucker and Schaeffel[21] (100 days)	Frozen tissue	85	293	2049	572	223	3340
Remtulla and Hallett[31]* (98–203 days)	Frozen tissue	93 ± 4	452 ± 8	203 ± 2	558 ± 20	237 ± 13	3372
Zhou et al.[36] (29 days)	OCT	90.8 ± 4.6	311.7 ± 18.1	1558.7 ± 18	707.4 ± 21.4	186.9 ± 15.1	3003.3 ± 44.1
Puk et al.[37] (11 weeks)	OCT	72.47–130.87	473–581	1999–2149			3430–3622
Zhou et al.[36] (67 days)	OCT	114 ± 7	370 ± 13	1734 ± 29	651 ± 24	187 ± 16	3233 ± 30
Tkatchenko et al.[14] (67 days)	MRI		381 ± 3	1940 ± 24	908 ± 36		3246 ± 3
Cone et al.[10] (6–12 weeks)	Fresh tissue						3430–3680 ± 100
Wang et al.[38] (8 weeks)	OCT	113 ± 4.6	413.3 ± 7.4	1783.4 ± 15.5	643.3 ± 14.8	205.2 ± 13.7	3158.2 ± 21.6
B6, 6–7 Months							
Present results	OCT	121 ± 7	430 ± 22	2016 ± 23	521 ± 31	215 ± 9	3303 ± 36
Remtulla and Hallett[28]* (98–203 days)	Frozen section	93 ± 4	452 ± 8	2032 ± 21	558 ± 20	237 ± 13	3372
D2, 2–3 Months							
Present results	OCT	122 ± 9	351 ± 27	1906 ± 29	606 ± 37	191 ± 13	3069 ± 43
Cone et al.[10] (6–12 weeks)	Fresh tissue						3350–3500 ± 80–100
D2, 12–14 Months							
Present results	OCT	111 ± 9	752 ± 27	2180 ± 29	600 ± 37	185 ± 11	3827 ± 43
Cone et al.[10] (50 weeks)	Fresh tissue						3830 ± 230

* Data are expressed as the mean ± SE in micrometers. All other data are the mean ± SD in micrometers. Empty cells indicate that data were unavailable.

(23.93 × IOP [mm Hg]). This model accounted for 73% of the total variance.

Figure 6 shows the changes in CC with increasing age. In the B6 mice, the CC tended to increase between 2 and 6 months of age and then remained at an approximately constant level. In the D2 mice, CC was more variable. There was a trend toward an increase until 8 months of age, followed by a trend toward a decrease after 10 months. The variability in the D2 mice appears to be due, at least in part, to changes in the anterior corneal radius caused by calcification.[11] An example is given for a 20-month-old D2 mouse (Fig. 7C). In this mouse, irregularities in corneal shape did not prevent precise measurement of the radius of curvature. Also note in Figure 7B the asymmetrically increased CT. Two-way ANOVA revealed signif-

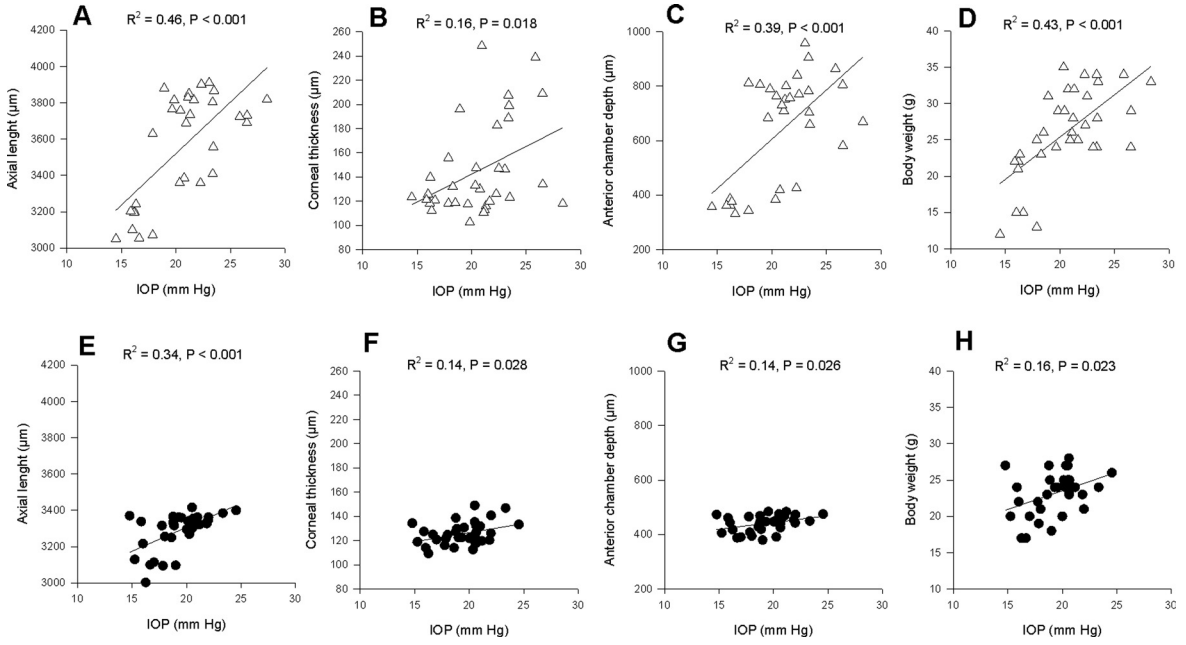

FIGURE 5. Relationship between IOP and relevant anatomic variables in D2 (**A–D**) and B6 (**E–H**) mice. *Solid lines*: linear regressions fitted to all data points.

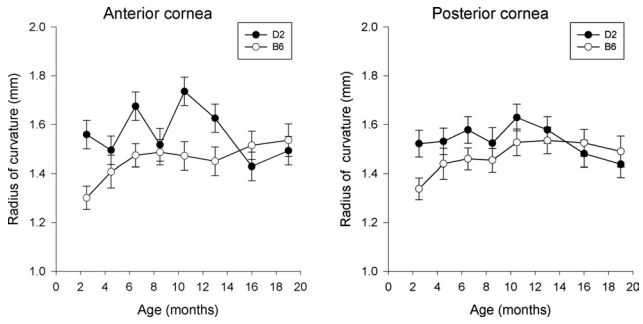

FIGURE 6. Curvature of the anterior and posterior cornea as a function of age in DBA/2J (D2) and C57BL/6J (B6) mice. Error bars, SEM.

icant effects of anterior CC with increased strain: $F_{(1,65)} = 14.48$, $P = <0.001$; age, $F_{(7,65)} = 2.26$, $P = 0.044$; and age × strain, $F_{(7,65)} = 2.72$, $P = 0.018$. The effects were less significant for the posterior CC (strain, $F_{(1,65)} = 5.44$, $P = 0.024$; age, $F_{(7,65)} = 1.63$, $P = 0.15$; and age × strain, $F_{(7,65)} = 1.11$, $P = 0.368$).

DISCUSSION

In this study we used a custom-built, whole-eye OCT system in a longitudinal investigation of postnatal changes in eye size in the well-known DBA/2J (D2) mouse model of glaucoma, which is characterized by spontaneous, long-standing IOP elevation. We focused on the changes in axial distances in the D2 mice and compared them with corresponding changes measured in the C57BL/6J (B6) mouse, a common control strain. We also tried to better understand the role of IOP elevation on eye size in D2 mice.

Altogether, the present results showed clear, progressive postnatal changes in all eye components in both the B6 and the D2 mice between 2 and 20 months of age. Although the AL was similar in the two strains in the age range 2 to 5 months, it increased relatively more in the D2 than in the B6 mice after 6 months of age and plateaued after 10 to 11 months. As it is known that, in D2 mice, IOP becomes elevated after 6 months of age and remains elevated thereafter, it is conceivable that exaggerated eye elongation is related to IOP elevation and exposure. A stronger correlation between IOP and AL in the D2 compared with the B6 mice, as well as an independent effect of IOP on AL established with multiple regression analysis, are consistent with this view. Another finding in support of the view that IOP played a role in abnormal eye elongation in the D2 mice is the exaggerated elongation of the anterior chamber compared with AL. Anterior chamber elongation as disease progresses in the D2 mice was previously reported by observation of slit lamp images.[24] Our results show that at approximately 8 months of age, there was a sharp elongation of the anterior chamber which was associated with a corresponding reduction in VCD. We interpret this finding as related to the fact that, at 8 months, IOP is known to substantially increase in D2 mice.[24,35,39] This change may result in a pressure gradient between the anterior and posterior chambers that tends to dislocate the lens posteriorly. At later ages, after 10 months of age, the pressure gradient between the anterior and posterior chambers may no longer be present, so that the lens tends to be pulled back to the original position, although it is unstable.

Starting at approximately 8 months of age, there were also substantial changes in CT in the D2 compared with the B6 mice, which included increases in thickness and thickness asymmetry. These may be caused by IOP elevation causing abnormal corneal hydration,[40] insufficiency of the corneal endothelium in removing excess fluid from the corneal stroma,[41] or a combination of both conditions. Protein accumulation may also occur in the aqueous humor of older D2 mice. Alteration of both CT thickness and aqueous humor protein content may be associated with changes in corresponding refractive indices,[42] resulting in one potential source of error in axial measurements. However, based on the data of Meek et al.,[42] the reduction in the refractive index in the extremely swollen corneas in our sample should have underestimated CT by only 7 μm. This effect should be counteracted by protein accumulation in the aqueous humor, which increases the refractive index.

Assuming that IOP is the primary cause of abnormal eye elongation, it should be taken into account that the time course of IOP changes may not precisely match that of AL changes due to the unknown role of compliance of eye tissues to eye pressure. In addition, there may be genetic factors that influence the rate and duration of eye elongation.[10,43] In this context, it is worth noting that IOP elevation in rat glaucoma models is not associated with an enlarged anterior chamber.[13] In summary, our data support the idea that elevated IOP plays a role in the exaggerated growth of eye size in D2 compared with B6 mice. However, a precise relationship between IOP and eye size cannot be firmly established because of a high degree of covariance between age, AL and IOP as well as the unknown role of tissue compliance on the mutual relationships among these variables.

Our data obtained with whole-eye OCT are in general agreement with previous measurements obtained with different methods, which are summarized in Table 2. Calkins et al.[17] used manganese-enhanced MRI to compare D2 and B6 mice of two different ages (2–3 months vs. 10–11 months) and reported that the ocular perimeter in the D2 mice (10–11 months) was approximately 12% larger than that in either the D2 or the B6 mice at 2 to 3 months. These authors also reported retinal thinning with increasing eye perimeter, as in the present study. Tkatchenko et al.,[14] used high-resolution MRI to study early postnatal changes in 2- to 3-month-old B6 mice. Our data are also in agreement with the postnatal changes in B6 mouse eye size previously reported in excised eyes.[7] The significantly larger size of the lens that we found in the D2 mice compared with that in the B6 mice is in good agreement with corresponding anatomic data on lens weight.[43] In vivo measurements in B6 mice have also been obtained with optical low-coherence interferometry. Schmucker and Schaeffel[21] used a system designed for human ocular biometry. This system provides distances in a single direction, and there is some uncertainly as to where the distance measurement is made. Zhou et al.,[22] used a custom-built, real-time OCT with a stepper motor to advance the focal plane from the cornea to the retina along the vertical axis. Images of the whole eye were reconstructed from multiple scans at different depths. Our whole-eye OCT system has the advantage that measurements of all eye components can be simultaneously determined. The system used in the present study relied on a time-domain implementation which has a limited

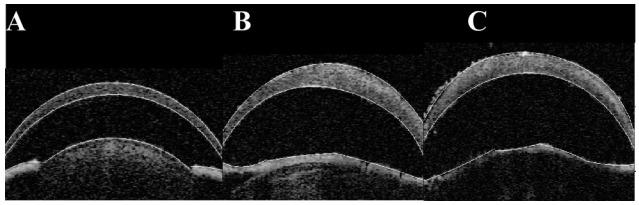

FIGURE 7. Examples of measurements of CC performed in DBA/2J mice at 2 (**A**), 8 (**B**), and 20 (**C**) months of age. Note in (**B**) the asymmetrically increased CT and in (**C**) the increased CT associated with irregularities of the corneal surface.

TABLE 3. Comparison of Corneal Radius of Curvature in B6 Mice of Different Ages between Different Laboratories and Instruments

Study (Mouse Age)	Method	Entire Cornea	Anterior Cornea	Posterior Cornea
B6, 2–3 Months				
Present results	Curve-fitting		1301 ± 76	1338 ± 81
Schmucker and Schaeffel[21] (100 days)	Frozen section		1493 ± 80	1415 ± 44
	Infrared photokeratometry		1414 ± 19	
Zhou et al.[22] (67 days)	Topcon keratometer	1503 ± 13		
Tkatchenko et al.[14] (67 days)	Calculated from AC depth/width	1483 ± 16		
B6, 6–7 Months				
Present results	Curve-fitting		1474 ± 40	1460 ± 37
Remtulla and Hallett[28*] (5 months)	Curve-fitting	1457 ± 85		1404 ± 74

* Data are expressed as the mean ± SE in micrometers. All other data are the mean ± SD in micrometers. Empty cells indicate that data were unavailable.

imaging speed. We and others have recently demonstrated that whole-eye images of the mouse can also be obtained with spectral-domain[44] or swept-source OCT.[38] These implementations allow image acquisition at much higher rates, which reduces the effect of eye movements and makes it possible to image the eye in three dimensions.

The values of the radius of curvature of B6 mice and its increase with age are consistent with previous results obtained with frozen sections[31] and keratometry.[7,36] (summarized in Table 3). Measurements from histologic sections seem to provide with our B6 results inlarger values,[45] probably due to histologic preparation artifacts. We found that there were only small differences between the anterior and posterior corneal radii of the B6 mice. This result is expected since the mouse cornea is very thin. We made the comparison of previous radius of curvature Table 3. The young D2 mice had a flatter cornea than did the B6 mice, whereas at older ages the reverse seemed to be true. The larger variability in the anterior CC of the D2 compared with the B6 mice seemed to be caused by the increasing irregularity in the shape of the D2. Irregularities of the corneal surface originate from keratic precipitates.[41] In agreement with our previous reports,[46] we found that precipitates had either an extrapupillary location, or involved the pupil area only minimally. It is unlikely that the presence of precipitates altered OCT measurements along the visual axis.

In the older D2 mice, the cornea became steeper (the radius of curvature became shorter). The steepening occurred in approximately the same age range as the increase in CT, plateau of AL, increase in ACD, and decrease in VCD. Corneal steepening associated with increased AL in the older D2 mice suggests development of myopia. All these concurrent phenomena may be associated with changes in IOP. It should be taken into account that the changes in CT and curvature observed in the older D2 mice may have substantially affected the accuracy of the IOP measurements, which we performed by rebound tonometry. Overall, the results show that there were baseline differences between the D2 and B6 mice as well as differences in the age dependence of the corneal shape.

The main advantages of OCT compared with MRI are its ease of use, fast acquisition time, and low cost. The fast acquisition time makes OCT suitable for routine use in large studies. On the other hand, unlike MRI, which can image the entire globe, OCT cannot image through strongly absorbant or scattering tissues, such as the sclera and iris. Another limitation of OCT compared to MRI is that the images must be corrected for optical distortions. First, the distances must be scaled by the refractive index. Second, refraction at the ocular boundaries produces distortions in the shape of the posterior structures—particularly the anterior chamber angle, lens, vitreous, and retina. The distortions make the posterior portions of the eye appear much flatter than they are in reality. With a flat scanning field, the anterior corneal distortions are negligible. Since the cornea of the mouse is thin, refraction of the light ray at the anterior surface does not produce significant distortions of the posterior surface. Optical distortions of the other structures can be corrected,[47–50] but there will always remain some uncertainty as to the error introduced. Another consequence of the refraction of light is that the lateral zone covered by the beam decreases as the beam propagates in the eye. The beam scans only a small fraction of the posterior lens surface and retina. It is possible to optimize the scan pattern to cover a larger area of the retina, but this would increase the complexity of the analysis.

In conclusion, using a custom-made whole-eye OCT, we demonstrated progressive changes in size of the different eye components with increasing age in DBA/2J mice and C57BL/6J mice, as well as differences between the two strains. Its fast acquisition time and noninvasiveness, together with ease of use and relative low-cost of the technology, makes whole-eye OCT suitable for routine use in longitudinal studies of mouse models of diseases involving changes in eye dimensions. The potential of our system appears to be particularly relevant in glaucoma models, as susceptibility to ocular elongation and retinal ganglion cell and axon damage among mice depends on several factors, including IOP, strain, and age.[10]

References

1. Pang IH, Clark AF. Rodent models for glaucoma retinopathy and optic neuropathy. *J Glaucoma.* 2007;16:483–505.
2. McKinnon SJ, Schlamp CL, Nickells RW. Mouse models of retinal ganglion cell death and glaucoma. *Exp Eye Res.* 2009;88:816–824.
3. Weinreb R, Lindsey J. The importance of models in glaucoma research. *J Glaucoma.* 2005;14:302–304.
4. Johnson TV, Tomarev SI. Rodent models of glaucoma. *Brain Res Bull.* 2010;81:349–358.
5. Chang B, Hawes NL, Hurd RE, Davisson MT, Nusinowitz S, Heckenlively JR. Retinal degeneration mutants in the mouse. *Vision Res.* 2002;42:517–525.
6. Elizabeth Rakoczy P, Yu MJ, Nusinowitz S, Chang B, Heckenlively JR. Mouse models of age-related macular degeneration. *Exp Eye Res.* 2006;82:741–752.
7. Schmucker C, Schaeffel F. A paraxial schematic eye model for the growing C57BL/6 mouse. *Vision Res.* 2004;44:1857–1867.
8. Zhou G, Williams RW. Mouse models for the analysis of myopia: an analysis of variation in eye size of adult mice. *Optom Vis Sci.* 1999;76:408–418.
9. Barathi VA, Beuerman RW, Schaeffel F. Effects of unilateral topical atropine on binocular pupil responses and eye growth in mice. *Vision Res.* 2009;49:383–387.

10. Cone FE, Gelman SE, Son JL, Pease ME, Quigley HA. Differential susceptibility to experimental glaucoma among 3 mouse strains using bead and viscoelastic injection. *Exp Eye Res.* 2010;91:415–424.
11. John SW, Smith RS, Savinova OV, et al. Essential iris atrophy, pigment dispersion, and glaucoma in DBA/2J mice (published correction in *Invest Ophthalmol Vis Sci*. 1998;39:1641). *Invest Ophthalmol Vis Sci*. 1998;39:951–962.
12. Brown AS, Zhang M, Cucevic V, Pavlin CJ, Foster FS. In vivo assessment of postnatal murine ocular development by ultrasound biomicroscopy. *Curr Eye Res.* 2005;30:45–51.
13. Nissirios N, Chanis R, Johnson E, et al. Comparison of anterior segment structures in two rat glaucoma models: an ultrasound biomicroscopic study. *Invest Ophthalmol Vis Sci.* 2008;49:2478–2482.
14. Tkatchenko TV, Shen YM, Tkatchenko AV. Analysis of postnatal eye development in the mouse with high-resolution small animal magnetic resonance imaging. *Invest Ophthalmol Vis Sci.* 2010;51:21–27.
15. Cheng H, Nair G, Walker TA, et al. Structural and functional MRI reveals multiple retinal layers. *Proc Natl Acad Sci U S A.* 2006;103:17525–17530.
16. Berkowitz BA, Roberts R, Goebel DJ, Luan H. Noninvasive and simultaneous imaging of layer-specific retinal functional adaptation by manganese-enhanced MRI. *Invest Ophthalmol Vis Sci.* 2006;47:2668–2674.
17. Calkins DJ, Horner PJ, Roberts R, Gradianu M, Berkowitz BA. Manganese-enhanced MRI of the DBA/2J mouse model of hereditary glaucoma. *Invest Ophthalmol Vis Sci.* 2008;49:5083–5088.
18. Duong TQ, Pardue MT, Thule PM, et al. Layer-specific anatomical, physiological and functional MRI of the retina. *NMR Biomed.* 2008;21:978–996.
19. Thuen M, Berry M, Pedersen TB, et al. Manganese-enhanced MRI of the rat visual pathway: acute neural toxicity, contrast enhancement, axon resolution, axonal transport, and clearance of Mn(2+). *J Magn Reson Imaging.* 2008;28:855–865.
20. Schulz D, Iliev ME, Frueh BE, Goldblum D. In vivo pachymetry in normal eyes of rats, mice and rabbits with the optical low coherence reflectometer. *Vision Res.* 2003;43:723–728.
21. Schmucker C, Schaeffel F. In vivo biometry in the mouse eye with low coherence interferometry. *Vision Res.* 2004;44:2445–2456.
22. Zhou X, Xie J, Shen M, et al. Biometric measurement of the mouse eye using optical coherence tomography with focal plane advancement. *Vision Res.* 2008;48:1137–1143.
23. Ruggeri M, Kocaoglu OP, Uhlhorn S, et al. Small animal ocular biometry using optical coherence tomography. *Proc SPIE*. 2010:7550:16.
24. Libby RT, Anderson MG, Pang IH, et al. Inherited glaucoma in DBA/2J mice: pertinent disease features for studying the neurodegeneration. *Vis Neurosci.* 2005;22:637–648.
25. Howell GR, Libby RT, John SWM. Mouse genetic models: an ideal system for understanding glaucomatous neurodegeneration and neuroprotection. *Prog Brain Res.* 2008:303–321.
26. Uhlhorn SR, Borja D, Manns F, Parel JM. Refractive index measurement of the isolated crystalline lens using optical coherence tomography. *Vision Res.* 2008;48:2732–2738.
27. Kocaoglu OP, Uhlhorn SR, Hernandez E, et al. Simultaneous fundus imaging and optical coherence tomography of the mouse retina. *Invest Ophthalmol Vis Sci.* 2007;48:1283–1289.
28. Remtulla S, Hallett PE. A schematic eye for the mouse, and comparisons with the rat. *Vision Res.* 1985;25:21–31.
29. Hughes A. A schematic eye for the rat. *Vision Res.* 1979;19:569–588.
30. Danias J, Kontiola AI, Filippopoulos T, Mittag T. Method for the noninvasive measurement of intraocular pressure in mice. *Invest Ophthalmol Vis Sci.* 2003;44:1138–1141.
31. Wang. Noninvasive measurement of rodent intraocular pressure with a rebound tonometer (published correction in *Invest Ophthalmol Vis Sci.* 2006;47:1268). *Invest Ophthalmol Vis Sci.* 2005;46:4617–4621.
32. Zhou XH, Li F, Kong L, Tomita H, Li C, Cao W. Involvement of inflammation, degradation, and apoptosis in a mouse model of glaucoma. *J Biol Chem.* 2005;280:31240–31248.
33. Porciatti V, Nagaraju M. Head-up tilt lowers IOP and improves RGC dysfunction in glaucomatous DBA/2J mice. *Exp Eye Res.* 2010;90:452–460.
34. Pease ME, Hammond JC, Quigley HA. Manometric calibration and comparison of TonoLab and TonoPen tonometers in rats with experimental glaucoma and in normal mice. *J Glaucoma.* 2006;15:512–519.
35. Pease ME, Cone FE, Gelman S, Son JL, Quigley HA. Calibration of the TonoLab tonometer in mice with spontaneous or experimental glaucoma. *Invest Ophthalmol Vis Sci.* 2011;52:858–864.
36. Zhou XT, Shen MX, Xie J, et al. The development of the refractive status and ocular growth in C57BL/6 mice. *Invest Ophthalmol Vis Sci.* 2008;49:5208–5214.
37. Puk O, Dalke C, Favor J, de Angelis JH, Graw J. Variations of eye size parameters among different strains of mice. *Mamm Genome.* 2006;17:851–857.
38. Wang L, Hofer B, Chen YP, Guggenheim JA, Drexler W, Povazay B. Highly reproducible swept-source, dispersion-encoded full-range biometry and imaging of the mouse eye. *J Biomed Opt.* 2010;15:046004.
39. Scholz M, Buder T, Seeber S, Adamek E, Becker CM, Lütjen-Drecoll E. Dependency of intraocular pressure elevation and glaucomatous changes in DBA/2J and DBA/2J-Rj mice. *Invest Ophthalmol Vis Sci.* 2008;49:613–621.
40. Foster CS, Azar D, Dohlman CH. *Smolin and Thoft's The Cornea; Scientific Foundations and Clinical Practice.* 4th ed. Philadelphia: Lippincott, Williams & Wilkins; 2005.
41. Chang B, Smith RS, Hawes NL, et al. Interacting loci cause severe iris atrophy and glaucoma in DBA/2J mice. *Nat Genet.* 1999;21:405–409.
42. Meek KM, Dennis S, Khan S. Changes in the refractive index of the stroma and its extrafibrillar matrix when the cornea swells. *Biophys J.* 2003;85:2205–2212.
43. Zhou G, Williams RW. *n*gene loci that modulate eye size, lens weight, and retinal area in the mouse. *Invest Ophthalmol Vis Sci.* 1999;40:817–825.
44. Ruggeri M, Uhlhorn S, Manns F, Parel J-M, Porciatti V. Whole eye imaging of small animals with spectral domain optical coherence tomography. *EOS Topical Meeting*: *5th European Meeting on Visual and Physiological Optics (EMVPO)*. Stockholm, Sweden, 22–24 August 2010, Royal Institute of Technology; 2010.
45. Smith RS, Korb D, John SW. A goniolens for clinical monitoring of the mouse iridocorneal angle and optic nerve. *Mol Vis.* 2002;8:26–31.
46. Porciatti V, Saleh M, Nagaraju M. The pattern electroretinogram as a tool to monitor progressive retinal ganglion cell dysfunction in the DBA/2J mouse model of glaucoma. *Invest Ophthalmol Vis Sci.* 2007;48:745–751.
47. Ortiz S, Siedlecki D, Grulkowski I, et al. Optical distortion correction in optical coherence tomography for quantitative ocular anterior segment by three-dimensional imaging. *Opt Express.* 2010;18:2782–2796.
48. Podoleanu A, Charalambous I, Plesea L, Dogariu A, Rosen R. Correction of distortions in optical coherence tomography imaging of the eye. *Phys Med Biol.* 2004;49:1277–1294.
49. Zawadzki RJ, Leisser C, Leitgeb R, Pircher M, Fercher AF. Three-dimensional ophthalmic optical coherence tomography with a refraction correction algorithm. *Proc SPIE*. 2003:5140:20–27.
50. Westphal V, Rollins A, Radhakrishnan S, Izatt J. Correction of geometric and refractive image distortions in optical coherence tomography applying Fermat's principle. *Opt Express.* 2002;10:397–404.